Journal of
Marine Science and Engineering

MDPI

Article

Dynamic Response and Multi-Objective Optimization of Lazy-Wave Dynamic Cables for Large-Capacity Floating Wind Turbines in Shallow Water

Mingda Ma * and Yangyang Gao

Ocean College, Zhejiang University, Zhoushan 316000, China
* Correspondence: 22334135@zju.edu.cn

Abstract

Dynamic cables, serving as the critical link between floating wind turbines and submarine cables, are subjected to significant tension fluctuations and bending deformations under environmental loading. While deep-water systems have been widely studied, investigations of large-capacity wind turbines in shallow water environments remain limited. This study establishes a coupled numerical model of an IEA 15 MW floating wind turbine and its dynamic cable system at a water depth of 50 m. The platform's six-degree-of-freedom motions were calculated under 0°, 90°, and 180° loading directions, followed by a systematic analysis of lazy-wave dynamic cable response characteristics. Results indicate that platform motions and dynamic cable responses are strongly direction-dependent in shallow water, with the 0° loading direction identified as the governing design case due to peak curvature and tension levels. Analysis reveals that the touchdown point location is the primary driver of tension response, while cable length increments predominantly influence bending. Utilizing these insights, a multi-objective fitness function was integrated with a Particle Swarm Optimization (PSO) algorithm. The optimized configuration significantly reduced peak curvature and total cable length, providing a theoretical framework and engineering guidance for the design of high-capacity floating wind systems in shallow-water regions.

Keywords: dynamic power cable; floating offshore wind turbine; lazy-wave configuration; particle swarm optimization; optimization

Check for updates

Academic Editor: Constantine Michailides

Received: 11 March 2026
Revised: 14 April 2026
Accepted: 15 April 2026
Published: 18 April 2026

Copyright: © 2026 by the authors. Licensee MDPI, Basel, Switzerland. This article is an open access article distributed under the terms and conditions of the Creative Commons Attribution (CC BY) license.

1. Introduction

Offshore wind energy, a renewable power source, has attracted significant interest for its minimal land footprint, abundant wind resources, and great potential for large-scale development [1]. However, as nearshore sites become increasingly saturated, offshore wind development is gradually shifting toward deep and ultra-deep waters. This transition requires a shift from traditional fixed-bottom structures to floating foundations. Projections suggest that by 2050, floating offshore wind will account for 5–15% of the total global offshore wind capacity [2]. Despite this optimistic outlook, floating offshore wind turbines (FOWTs) still face several key technical challenges [3]. Principal among these is ensuring the long-term reliability and integrity of the power transmission system [4]. Historical data indicates that the majority of operational downtime and associated economic losses in offshore projects stem from submarine cable failures [5,6]. Unlike conventional static cables, dynamic power cables connect a floating turbine to submarine cables. Their mid-span

segments are suspended in the water column and subjected to complex dynamic loads induced by wind, waves, currents, and platform motions. These persistent cyclic loads make the cables particularly susceptible to fatigue damage [7], which necessitates a rigorous analysis of their dynamic response.

Extensive research has been devoted to the configuration and dynamic response of dynamic cables. In terms of dynamic behavior of dynamic cables, Martinelli et al. [8] conducted scaled model tests at a water depth of 100 m to investigate the dynamic behavior of catenary and lazy-wave dynamic cables, demonstrating that the introduction of buoyancy modules effectively reduces loads in the suspended cable segments. Zhao et al. [9] compared lazy-wave and double-wave configurations for 5 MW turbines in shallow water, finding that double-wave designs improved curvature control, though long-term fatigue remains under-explored. Beier et al. [10] analyzed the fatigue life of cables for 5 MW floating turbines at a water depth of 200 m, showing that bending stress is the dominant factor inducing fatigue damage. Ahmad et al. [11] proposed configuration optimizations for dynamic cables in 5 MW floating turbine arrays at a water depth of 320 m, demonstrating that small buoyancy modules promote uniform tension. Guo et al. [12] performed dynamic and fatigue analyses of dynamic cables, showing that increasing cable mass and modifying suspension angles effectively reduces curvature. Ericka et al. [13] designed lazy-wave dynamic cables for floating wind turbines at water depths of 800 m, 200 m, and 80 m, and analyzed the effective tension and curvature of the dynamic cables. Anna et al. [14] conducted scaled model tests of dynamic cables for floating wind turbines at a water depth of 70 m, showing that the dynamic response of dynamic cables is significantly influenced by the motion of the floating turbine.

In terms of structural optimization of dynamic cables, Rentschler et al. [15] utilized genetic algorithms at water depths of 70–200 m, reducing the buoyant segment length to 18–23% of the total cable length. Schnepf et al. [16] employed long short-term memory neural networks to optimize dynamic cable configurations for 5 MW floating turbines at a depth of 320 m, achieving a significant reduction in total cable length. Zhao X et al. [17] proposed a machine-learning framework for lazy-wave dynamic cables at a water depth of 119.5 m, achieving an 18.3% reduction in maximum curvature while satisfying tension constraints. Zhao B et al. [18] analyzed the effective tension and bending curvature of dynamic cables at a water depth of 100 m under various design loads, and developed a connection optimization scheme based on fracture morphology, demonstrating that the ultimate load-bearing capacity increased by 17.5% after optimization. Wang et al. [19] proposed a stepwise optimization method for lazy-wave dynamic cables using a mass-damping equivalent model, achieving complex multi-objective optimization progressively under still water, regular wave, and random wave conditions.

In summary, existing research primarily focuses on deep-water environments or small-capacity turbines. Systematic investigations into lazy-wave cables for large-capacity turbines in shallow-water environments remain limited. The influence of key parameters, such as the touchdown point location and total cable length, on tension and curvature has not been fully elucidated. To address this gap, the present study develops a coupled numerical model of an IEA 15 MW floating wind turbine and dynamic cable at a water depth of 50 m. First, the motion response characteristics of the floating platform under extreme conditions are analyzed. On this basis, the dynamic response behavior of the dynamic cable is investigated to reveal the influence of cable length and touchdown point position on tension and curvature responses. Furthermore, a Particle Swarm Optimization (PSO) method is introduced to optimize the lazy-wave dynamic cable configuration.

2. Structural Parameters

This study employs the IEA 15 MW reference wind turbine developed by the International Energy Agency (NREL, Golden, CO, USA). The turbine features a rotor radius of 120 m, a tower length of 139.5 m, and a hub height of 150 m. This model has been widely adopted in floating wind turbine dynamics research; its primary parameters are detailed in Table 1.

Table 1. Key Parameters of the IEA 15 MW Wind Turbine [20].

Parameter	Value	Unit
Rated Power	15	MW
Rotor Diameter	240	m
Hub Diameter	7.94	m
Hub Height	150	m
Cut-in Wind Speed	3	m/s
Rated Wind Speed	10.59	m/s
Cut-out Wind Speed	25	m/s
Tower Mass	1263	t
RNA Mass	991	t

The floating wind turbine is designed for a deployment site with a water depth of 50 m, utilizing the VolturnUS-S semi-submersible foundation. The foundation has a total length of 102.13 m, a width of 90.13 m, and a height of 35 m, with a draft of 20 m and a total mass of 17,854 t; its primary parameters are detailed in Table 2.

Table 2. Key Parameters of the VolturnUS-S semi-submersible foundation [21].

Parameter	Value	Unit
Platform type	semi-submersible	-
Displacement	20,206	m^3
Length	90.13	m
Width	102.13	m
Height	290.00	m
Freeboard	15	m
Draft	20	m
Vertical center of gravity from SWL	−14.95	m
Vertical center of buoyancy from SWL	−13.63	m
Total mass	20,108	t
Platform mass	17,854	t

The mooring system consists of nine catenary lines in a 3 × 3 symmetric configuration. The fairleads are located 10 m above the waterline, with an anchor radius of 500 m. The specific mooring parameters are listed in Table 3.

For offshore wind turbines above 10 MW, 66 kV flexible cables have become the mainstream power collection method [23]. In this study, a 66 kV double-armored three-core dynamic cable is adopted, and its cross-sectional structure is shown in Figure 1.

The cable structure includes the conductor core, filling, inner sheath, armor layer, and outer sheath. Buoyancy modules are integrated to maintain the lazy-wave configuration, ensuring that curvature and tension requirements are met under operating conditions. Detailed cable parameters are provided in Table 4. The bending curvature limit of 0.455 and tension limit of 599 kN of the dynamic cable adopted in this study were provided by the cable manufacturer in accordance with CIGRE TB862 [24] and CIGRE TB623 [25].

Table 3. Key Parameters of the Mooring System [22].

Parameter	Value	Unit
Mooring Type	Catenary	-
Chain Grade	R4 Studless	-
Number of Lines	9	-
Mooring Radius	500	m
Anchor Depth	50	m
Fairlead Height	10	m
Chain Diameter	0.210	m
Dry Weight	0.878	t/m
Axial Stiffness	3,770,000	kN
Breaking Strength	32,880	kN
Fairlead Pre-tension	1098	kN

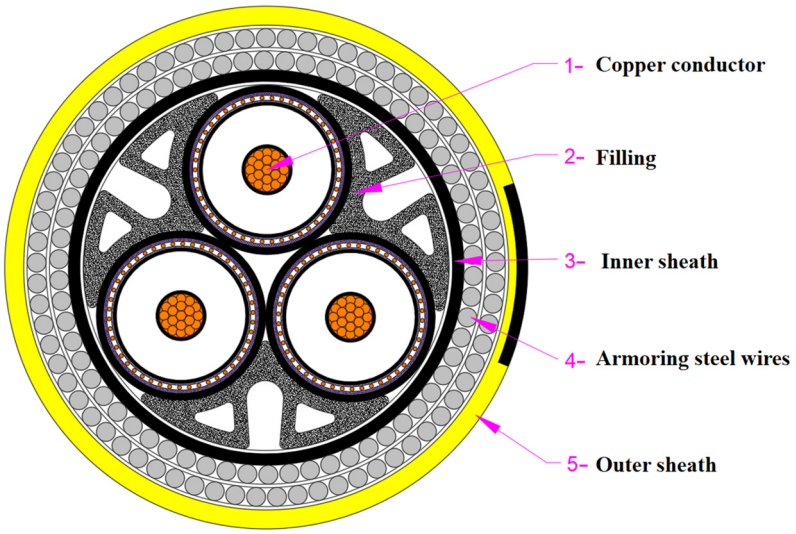


Figure 1. Cross-sectional structure of the cable.

Table 4. Key Parameters of the Dynamic Cable.

Parameter	Value	Unit
Outer Diameter	0.1513	m
Dry Weight	0.396	kN/m
Bending Stiffness	14.1	kN·m^2
Axial Stiffness	575.5	MN
Torsional Stiffness	97.5	kN·m^2
Maximum Tension	599	kN
Minimum Bending Radius	2.2	m
Floater Outer Diameter	0.63	m
Floater Length	1	m
Buoy Spacing	4	m
Net Buoyancy	1.88	kN

According to the characteristics of the lazy-wave configuration, the cable is divided into three distinct segments: the hang-off section L_1, the buoyancy section L_2 and the touchdown section L_3, with the total cable length represented by L. Drawing on the findings of Rentschler et al. [15], a segment length ratio of $L_1 : L_2 : L_3 = 1 : 1 : 2$ was adopted. At the design water depth of $d = 50$ m, the hang-off point is positioned $H = 30$ m above the seabed. The touchdown point is established on the leeward side of the turbine,

located at a horizontal distance D from the vertical projection of the hang-off point, as shown in Figure 2.

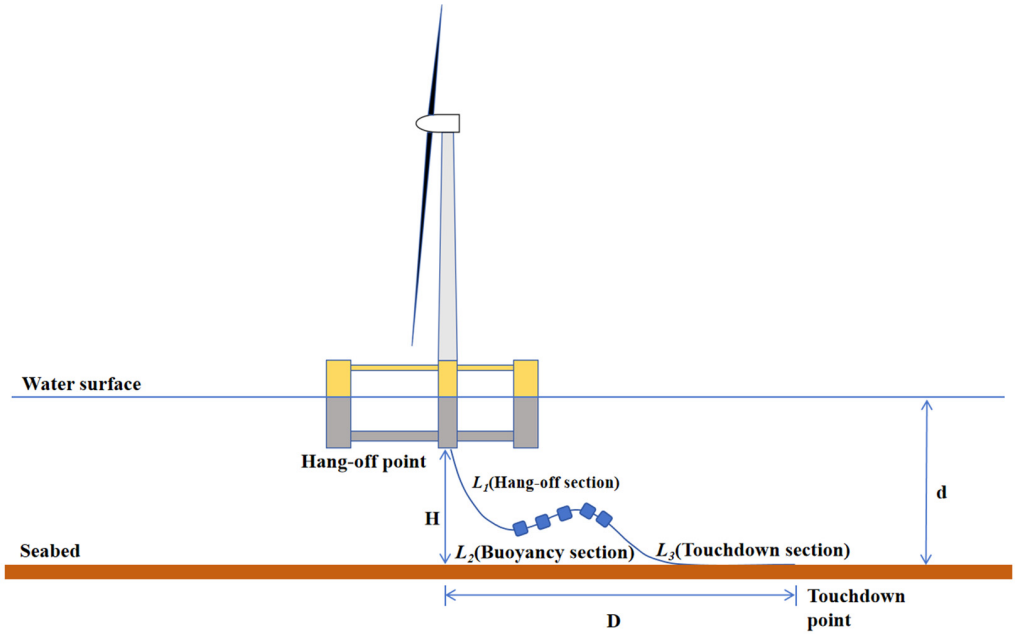


Figure 2. Schematic layout of the lazy-wave dynamic cable.

3. Calculation Theory

3.1. Lazy-Wave Configuration

The mechanical characteristics of a dynamic cable are typically investigated in two sequential stages: static analysis and dynamic analysis. The catenary method is commonly applied during the static analysis phase due to its clear physical interpretation and computational efficiency. The lazy-wave configuration assumes the dynamic cable is homogeneous, flexible, and inextensible. By introducing distributed buoyancy modules into a traditional catenary structure, the dynamic cable forms a spatial configuration similar to a wave profile. As shown in Figure 3, ω_s represents the submerged weight per unit length of the cable, and ω_b is the net buoyancy per unit length of the buoyancy section. T_v and T_h are the vertical and horizontal tension components at the hang-off point, respectively. X_1, X_2, and X_3 are the horizontal projections of each segment, while Z_1, Z_2, and Z_3 denote their respective vertical heights. The angle θ_1 is the declination angle at the hang-off point; θ_2 and θ_3 are the tangent angles at the segment junctions; and θ_4 is the tangent angle at the touchdown point. The length of the hang-off section is L_1, the length of buoyancy section is L_2 and the length of touchdown section is L_3. The total cable length represented by L.

The tension at the hang-off point can be expressed as:

$$T_v = \omega_s(L_1 + L_3) + \omega_b L_2 \tag{1}$$

$$T_h = \frac{T_v}{tan\theta_1} \tag{2}$$

The following series of equations are derived to solve the lazy-wave geometry:

$$\theta_3 = tan^{-1}(tan\theta_4 + \frac{\omega_s L_3}{T_h}) \tag{3}$$

$$\theta_2 = tan^{-1}(\frac{\omega_b L_2 + T_h tan\theta_3}{T_h}) \tag{4}$$

$$\theta_1 = tan^{-1}\left(\frac{\omega_s L_1 + T_h tan\theta_2}{T_h}\right) \tag{5}$$

Based on classical catenary theory, the force analysis of a segment yields:

$$T\sin\theta = T_v = \omega_s L \tag{6}$$

$$T\cos\theta = T_h \tag{7}$$

$$\tan\theta = \frac{T_v}{T_h} = \frac{\omega_s L}{T_h} \tag{8}$$

Taking a differential element along the catenary:

$$dL = \left(1 + \tan^2\theta\right)(dX)^2 = \left[1 + \left(\frac{\omega_s L}{T_v}\right)^2\right](dX)^2 \tag{9}$$

$$dX = \frac{dL}{\sqrt{1 + \left(\frac{\omega_s L}{T_h}\right)^2}} \tag{10}$$

$$dZ = \frac{\frac{\omega_s L}{T_h} dL}{\sqrt{1 + \left(\frac{\omega_s L}{T_h}\right)^2}} \tag{11}$$

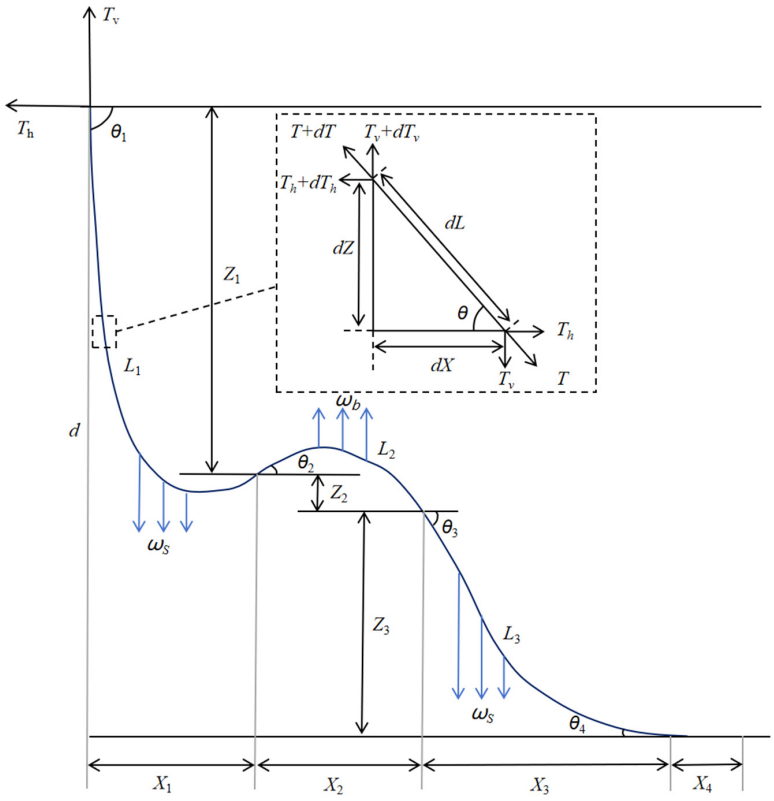


Figure 3. Design parameters for the lazy-wave configuration.

Integrating Equations (10) and (11) results in the following expressions for the horizontal and vertical projections:

$$X = \frac{T_h}{\omega_s} \ln\left(\sqrt{1 + \left(\frac{\omega_s L}{T_h}\right)^2} + \frac{\omega_s L}{T_h}\right) \tag{12}$$

$$Z = \frac{T_h}{\omega_s}\sqrt{1+\left(\frac{\omega_s L}{T_h}\right)^2} - \frac{T_h}{\omega_s L} \tag{13}$$

Simplifying these equations leads to the following expressions:

$$L = \sqrt{Z^2 + \frac{2T_h Z}{\omega_s}} \tag{14}$$

$$T = \sqrt{{T_h}^2 + (\omega_s L)^2} = T_h\sqrt{\left(\frac{\omega_s L}{T_h}\right)^2 + 1} = T_h + \omega_s Z \tag{15}$$

$$X = \frac{T_h}{\omega_s}\sinh^{-1}\left(\frac{\omega_s L}{T_h}\right) \tag{16}$$

Combining Equations (1)–(16) allows the calculation of the horizontal projections X_1, X_2, and X_3 and the key heights Z_1, Z_2, and Z_3.

3.2. Lumped Mass Method

The lumped mass method discretizes the dynamic cable into a series of nodes connected by massless line segments. The nodes represent the physical properties of the dynamic cable, including mass, weight, and buoyancy. The segments utilize axial, bending, and torsional springs, along with corresponding dampers, to simulate the tensile, bending, and torsional characteristics of the dynamic cable, as illustrated in Figure 4. This method accounts for the hydrodynamic forces and elastic deformations experienced by the cable. Compared to the finite element method, it offers good computational accuracy and significantly higher computational efficiency, which has led to its widespread adoption.

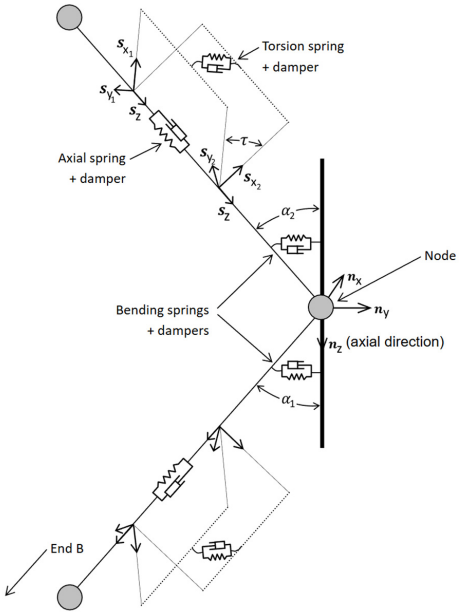


Figure 4. Schematic of the lumped mass method.

3.3. Effective Tension and Bending Curvature

Under the influence of hydrostatic pressure, the effective tension of the dynamic cable is calculated as follows:

$$T_e = T_w + (1-2v)p_0 A_0 + EAe(dL/dt)/L_0 \tag{17}$$

where T_e is the effective tension and T_w is the wall tension ($T_w = EA\varepsilon$). In this expression, ν denotes the Poisson's ratio, p_0 represents the external pressure, A_0 is the cross-sectional area of the cable, and EA is the axial stiffness. The parameter e refers to the cable damping coefficient, dL/dt is the rate of length increase, L_0 is the initial length of the cable element, and ε is the total average axial strain.

The bending angle of the dynamic cable element is defined as the angle between the element axis S_z and the node axis n_z, from which the effective curvature κ of the cable can be derived. The expression for the bending moment is given by:

$$M = EI\kappa + (\lambda_t/100)D_c \cdot d\kappa/dt \tag{18}$$

where EI is the bending stiffness of the dynamic cable, λ_t is the target bending damping, D_c is the critical bending damping value, and $d\kappa/dt$ represents the rate of change in the curvature.

3.4. Particle Swarm Optimization

Particle Swarm Optimization (PSO) is a stochastic optimization method based on swarm intelligence. It functions by constructing a search population composed of multiple "particles" that collaboratively search for the optimal solution within a solution space. Each particle represents a potential solution and continuously adjusts its search direction by tracking its own historical best position and the global best position of the entire swarm, thereby achieving iterative optimization of the objective function. The Particle Swarm Optimization algorithm does not rely on gradient information of the objective function; it updates the search direction solely by comparing fitness values, which gives it strong applicability [26]. Its population-based collaborative mechanism endows the algorithm with robust global search capability. Furthermore, PSO involves only a few control parameters, such as population size, inertia weight, acceleration coefficients, maximum number of iterations, and fitness tolerance, making it easy to implement. Therefore, this study adopts the PSO algorithm for the optimization of dynamic cables. In each iteration, the velocity and position of a particle are updated based on their values from the previous time step. Let $V_i(t)$ and $X_i(t)$ denote the velocity and position of particle i at time t, respectively. The update formulas for velocity and position at time step $t + 1$ are as follows:

$$V_i(t+1) = wV_i(t) + c_1r_1(pBest_i(t) - X_i(t)) + c_2r_2(gBest_i(t) - X_i(t)) \tag{19}$$

$$X_i(t+1) = X_i(t) + V_i(t) \tag{20}$$

where $V_i(t+1)$ is the velocity of particle i at time $t + 1$, and $X_i(t+1)$ is the position of particle i at time $t + 1$. The parameter w is the inertia weight, representing the confidence in the current velocity direction; c_1 and c_2 are learning factors used to adjust the maximum step size; r_1 and r_2 are random values in the range [0, 1] used to enhance search stochasticity; $pBest_i(t)$ is the historical best position of particle i at time t, and $gBest_i(t)$ is the global best position of particle i at time t.

4. Results and Discussion

4.1. Motion Response Characteristics of the Floating Wind Turbine

The motion of the floating platform defines the boundary conditions at the hang-off point of the dynamic power cable, directly influencing its tension and curvature characteristics. Therefore, analyzing the platform's motion is a prerequisite for evaluating the response of the dynamic cable. To obtain the motion response under extreme environmental conditions, a coupled numerical model of the floating wind turbine and dynamic cable

was established using the professional hydrodynamic software OrcaFlex 11.4, as shown in Figure 5.

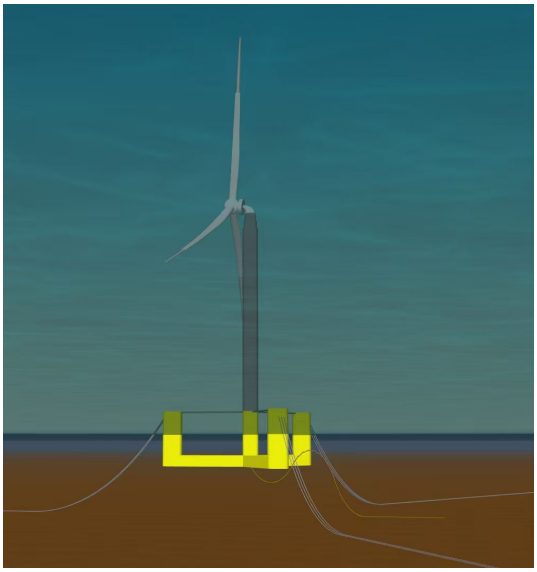


Figure 5. Schematic of the coupled numerical model for the floating wind turbine and dynamic cable.

This study references the OrcaFlex official K03 example model and establishes a floating wind turbine model using the IEA 15 MW turbine and the VolturnUS-S platform. This model has been cross-validated between OrcaFlex and OpenFAST (v3.3), ensuring the accuracy of the turbine-platform modeling. The dynamic cable parameters are set following reference [14]: the drag coefficient is based on OrcaFlex's built-in Reynolds-dependent variable drag coefficient; the added mass coefficients are selected according to DNVGL-OS-C101 [27] and DNV-RP-C205 [28], with a normal coefficient of 1.0 and an axial coefficient of 0.05. The top end of the dynamic cable is connected to the floating platform, and its bottom end is anchored to the seabed, with a discretization element length of 0.1 m. The numerical simulations employ the implicit integration algorithm, which is recommended by OrcaFlex. The simulation time duration for each case is 3600 s with a time step of 0.05 s.

In this study, dynamic analysis of a floating offshore wind turbine's dynamic cable under extreme sea conditions is carried out. The extreme sea condition parameters are derived from in situ measurements at an offshore wind farm site in the South China Sea and are listed as follows: the wind speed is 57 m/s at the hub height, the significant wave height $H_s = 10.4$ m, the peak period $T_p = 14.9$ s, the peak enhancement factor $\gamma = 3.3$, and the current velocity is 2.46 m/s.

The platform motion response is most significant under the three loading directions of 0°, 90°, and 180° [9]. Therefore, three cases were simulated with wind, wave, and current directions set to 0°, 90°, and 180°, as illustrated in Figure 6.

Under extreme conditions, the motion characteristics of the floating platform exhibit significant directional dependency. Figure 7 presents the 6-DOF motion time-series responses of the platform under different loading directions. The results indicate that surge and pitch are primarily driven by longitudinal loads, showing significant responses at 0° and 180°. Notably, the surge response is highest at 180°, reaching a peak value of −29.03 m, which is substantially greater than the maximum surge displacement of 18.11 m at 0°. This result is consistent with the findings of Ericka et al. [13], whose analysis of a 15 MW floating wind turbine also shows that the platform displacement under the 180° loading direction is greater than that under the 0° direction. The corresponding maximum pitch angles at 0° and 180° are 10.22° and −10.54°, respectively, indicating that surge is more sensitive

to the loading direction. Sway, roll, and yaw motions are mainly affected by transverse loads, with extreme values occurring under the 90° load direction. The maximum sway displacement reaches 23.27 m, roll angle is −8.14°, and yaw angle is 4.61°. Heave motion is less sensitive to the load direction, with a maximum displacement of −6.05 m. The extreme values of all platform degrees of freedom are summarized in Table 5, providing quantitative boundary conditions for the dynamic cable hang-off points.

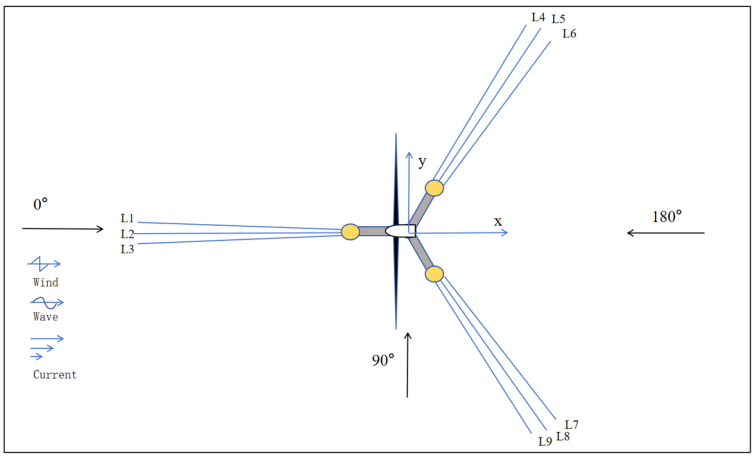
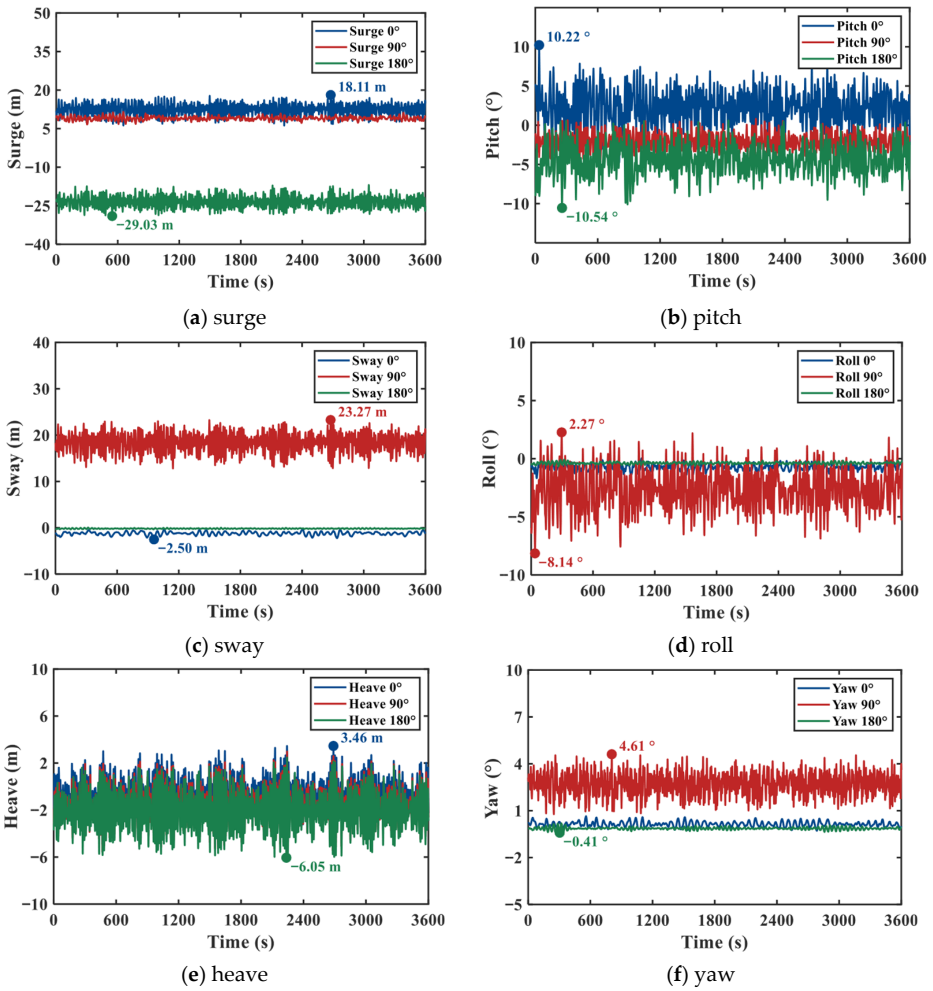


Figure 6. Schematic of different environmental loading directions.



(**a**) surge (**b**) pitch (**c**) sway (**d**) roll (**e**) heave (**f**) yaw

Figure 7. Time-series response curves of the 6-DOF motions of the floating wind turbine under various wind, wave, and current directions.

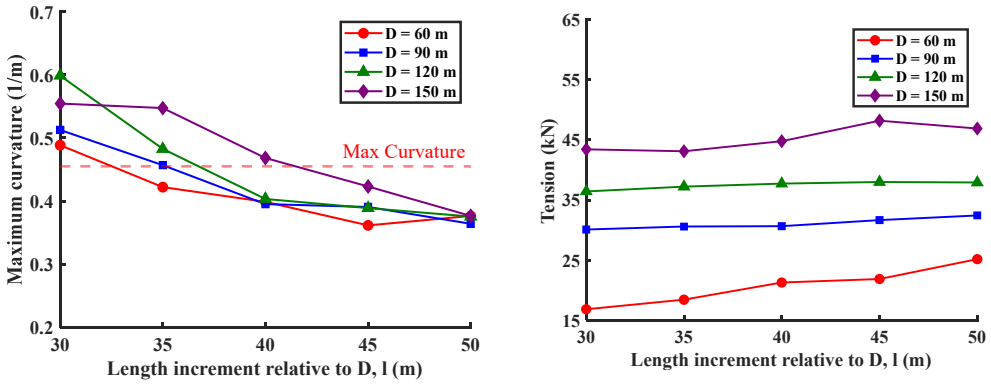
Table 5. Extreme motion responses (offsets) of the floating wind turbine platform.

Surge/m	Sway/m	Heave/m	Roll/°	Pitch/°	Yaw/°
−29.03	23.27	−6.05	−8.14	−10.54	4.61

4.2. Sensitivity Analysis of Dynamic Cable Configuration Parameters

The dynamic response characteristics of the lazy-wave dynamic cable were investigated under 0°, 90°, and 180° loading directions to evaluate the influence of cable length and touchdown position on its performance. This analysis provides the theoretical basis for subsequent structural optimization. In shallow-water conditions, if the horizontal distance D between the touchdown point and the hang-off point is too small, the geometric configuration of the lazy-wave dynamic cable is altered. This reduces or eliminates the slack section, leading to enhanced axial stretching effects and unfavorable structural responses. Therefore, D was set to values of $2H$, $3H$, $4H$ and $5H$, where H is the height of the hang-off point. The parameter l represents the cable length increment relative to distance D, with values of 30 m, 35 m, 40 m, 45 m, and 50 m.

Under the 0° loading direction, the maximum curvature and tension of the lazy-wave dynamic cable exhibit significant trends relative to the configuration parameters, as shown in Figure 8 and summarized in Table 6. The maximum curvature increases significantly with the touchdown distance D but decreases as the length increment l grows. When $l = 30$ m, the maximum curvature increases from 0.489 at $D = 60$ m to 0.599 at $D = 120$ m, an increase of 22%, and both values exceed the curvature limit of 0.455. In contrast, when $l = 50$ m, the maximum curvature increases only by 3%, from 0.364 at $D = 90$ m to 0.377 at $D = 150$ m. This is because, for a lazy-wave dynamic cable with a constant l, increasing D expands the sag range of the suspended section, making platform-induced displacements more likely to cause localized bending concentration and higher peak curvatures. Conversely, for a constant D, increasing l enhances the cable slackness, thereby mitigating the bending deformation caused by platform excursions. Notably, when $l = 30$ m, the maximum curvature in all cases exceeds the breaking curvature limit of 0.454 rad/m, indicating an insufficient safety margin when the cable length is short. Regarding tension response, the maximum tension increases with both D and l. When l is fixed at 50 m, the maximum tension increases from 25.17 kN to 46.90 kN as D increases, corresponding to a relative increase of approximately 86%. When D is fixed at 60 m, the maximum tension increases from 43.45 kN to 46.90 kN as l increases, with a change rate of only about 7%. This suggests that the touchdown point position has a more dominant influence on the axial tensile response than the cable length increment.



(**a**) maximum curvature (**b**) maximum tension

Figure 8. Variation curves of maximum curvature and maximum tension of the dynamic cable under 0° loading direction with respect to touchdown point distance D and length increment l.

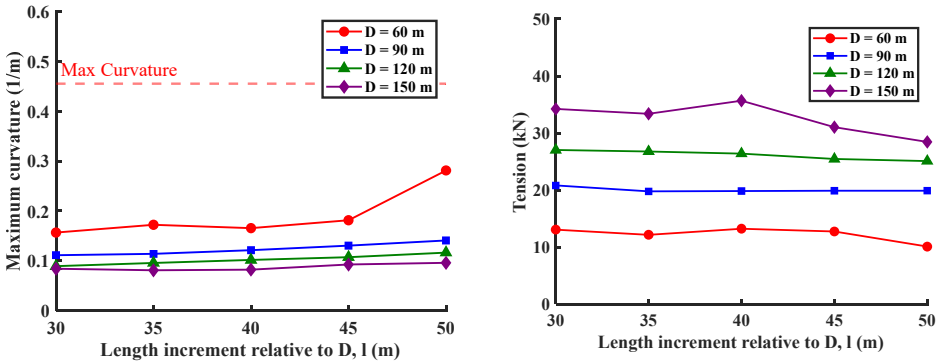
Table 6. Maximum curvature and tension of the dynamic cable for different touchdown point distances D and length increments l under 0° loading direction.

D (m)	l (m)	Maximum Curvature	Maximum Tension (kN)
60	30	0.489	16.82
	35	0.422	18.41
	40	0.399	20.82
	45	0.362	21.86
	50	0.376	25.17
90	30	0.513	30.10
	35	0.457	30.59
	40	0.395	30.65
	45	0.391	31.66
	50	0.364	32.45
120	30	0.599	36.44
	35	0.483	37.23
	40	0.403	37.73
	45	0.389	38.00
	50	0.375	37.92
150	30	0.555	43.45
	35	0.547	43.12
	40	0.468	44.79
	45	0.423	48.20
	50	0.377	46.90

Figure 9 illustrates the variation in maximum curvature and tension under the 90° loading direction. The corresponding extreme value statistics are presented in Table 7. While the maximum curvature tends to increase with both D and l, at $D = 60$ m and $l = 50$ m, the maximum curvature is 0.281, and the overall curvature level is significantly lower than that under the 0° loading condition. This is because, under lateral loading, the platform motion is dominated by sway and roll, which have a smaller impact on the cable's axial direction. Furthermore, the lateral environmental loads increase the axial tension of the cable, reducing the degree of bending and thus lowering peak curvature. As the touchdown point distance D increases, the length of the suspended section grows, increasing the lateral forces acting on the cable and leading to a significant rise in maximum tension; when $D = 60$ m, the maximum tension is 13.24 kN; when $D = 150$ m, the maximum tension is 35.65 kN. In contrast, the maximum tension shows minimal sensitivity to changes in the length increment l, confirming that the touchdown point position is the critical parameter governing tension response under 90° wind, wave, and current conditions.

Under the 180° loading direction, the variation in maximum curvature and tension with respect to D and l is shown in Figure 10 and summarized in Table 8. The maximum curvature exhibits a downward trend as the touchdown point distance D increases, while it increases slightly with the length increment l; when $D = 60$ m and $l = 50$ m, the curvature reaches its maximum value of 0.416, which is below the curvature limit. This occurs primarily because, under 180° loading, the longitudinal platform motion results in cable stretching, which suppresses the formation of slack zones and relatively weakens localized bending deformation. While the maximum tension increases with D, it gradually decreases as l rises. Specifically, at $l = 30$ m, increasing D from 60 m to 90 m reduces the maximum tension by approximately 96 kN, highlighting the significant regulatory effect of the TDP position on the tension response. It is worth noting that when $D = 60$ m, as l increases from 30 m to 35 m, the maximum tension decreases by 98.96 kN; the closer TDP makes the

lazy-wave dynamic cable geometric configuration more sensitive to platform excursions, resulting in a higher sensitivity of curvature and tension to parameter variations.



(**a**) maximum curvature (**b**) maximum tension

Figure 9. Variation curves of maximum curvature and maximum tension of the dynamic cable under 90° loading direction with respect to touchdown point distance D and length increment l.

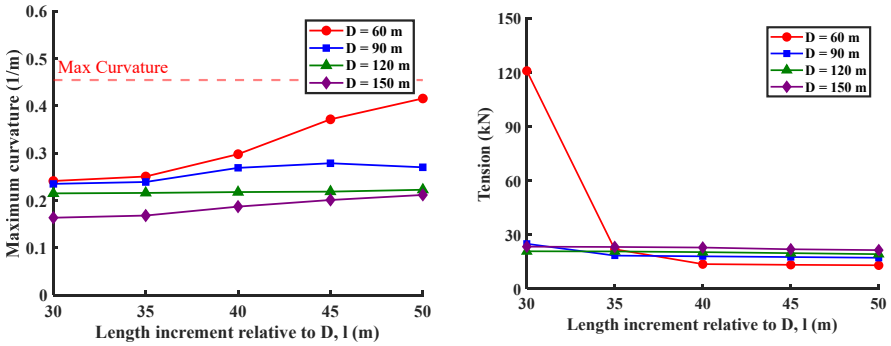
Table 7. Maximum curvature and tension of the dynamic cable for different touchdown point distances D and length increments l under 90° loading direction.

D (m)	l (m)	Maximum Curvature	Maximum Tension (kN)
60	30	0.157	13.08
	35	0.173	12.17
	40	0.166	13.24
	45	0.182	12.75
	50	0.281	10.10
90	30	0.112	20.81
	35	0.114	19.77
	40	0.122	19.84
	45	0.131	19.89
	50	0.141	19.9
120	30	0.090	27.02
	35	0.096	26.77
	40	0.102	26.39
	45	0.108	25.45
	50	0.117	25.09
150	30	0.084	34.21
	35	0.081	33.37
	40	0.083	35.65
	45	0.093	31.03
	50	0.096	28.45

Comparing the results across the three loading directions, it is evident that the loading direction directly dictates the platform's motion characteristics, significantly altering the kinematic constraints at the hang-off point and thereby affecting the bending and tensile response mechanisms.

In the 0° loading direction, longitudinal platform motion is most pronounced. This increases the reserve length of the cable, enhancing bending effects. Combined with the cable's self-weight and current drag, the tension fluctuations are significant, leading to overall higher maximum tension and curvature compared to other directions. In the 90° loading direction, the platform moves predominantly in the transverse direction. The cable remains in a more stretched state, significantly reducing curvature, although maximum tension is heavily influenced by hydrodynamic drag. In the 180° loading direction, the

reverse longitudinal motion maintains the cable in a tensioned state, reducing maximum curvature. Furthermore, the current alters the lazy-wave profile and reduces the suspended length, leading to a decrease in tension.



(**a**) maximum curvature (**b**) maximum tension

Figure 10. Variation curves of maximum curvature and maximum tension of the dynamic cable under 180° loading direction with respect to touchdown distance D and length increment l.

Table 8. Maximum curvature and tension of the dynamic cable for different touchdown point distance D and length increment l under 180° loading direction.

D (m)	l (m)	Maximum Curvature	Maximum Tension(kN)
60	30	0.241	121
	35	0.251	22.04
	40	0.298	13.75
	45	0.372	13.36
	50	0.416	13.1
90	30	0.235	25.06
	35	0.239	18.52
	40	0.269	18.13
	45	0.279	17.68
	50	0.270	17.27
120	30	0.215	20.87
	35	0.216	20.83
	40	0.218	20.38
	45	0.219	19.85
	50	0.223	19.32
150	30	0.164	23.48
	35	0.168	23.3
	40	0.187	22.95
	45	0.201	22.02
	50	0.212	21.5

Under the 0° loading direction, the maximum curvature of the dynamic cable is 0.599, significantly higher than those under the 90° direction and the 180° direction. Under the 180° loading direction, the maximum tension is 121 kN, exceeding those under the 0° direction and the 90° direction. Therefore, the 0° direction governs the curvature response, while the 180° direction governs the tension response. These findings are consistent with the results reported in [12,19].

Comparing the adopted dynamic cable limits, the tension limit is 599 kN, far above the maximum measured values under all loading directions. The curvature limit is 0.455, whereas the maximum curvature under the 0° direction is 0.599, which exceeds this limit. This agrees with the conclusion in [13] that "curvature is the governing parameter for

dynamic cables in shallow water". Consequently, within the selected parameter range, the 0° loading case is identified as the governing condition for the extreme response of the dynamic cable. All subsequent configuration optimization and fitness analyses are therefore based on the 0° loading direction.

To systematically evaluate the response characteristics under various parameter combinations and guide configuration optimization, a comprehensive assessment of maximum curvature and tension was performed. A fitness function is defined to evaluate the combined response:

$$F = \frac{T_{\max}}{T} + \frac{\rho_{\max}}{\rho} \tag{21}$$

where F is the fitness function, T_{max} is the maximum tension from motion analysis, T is the allowable tension, ρ_{max} is the maximum curvature from analysis, and ρ is the allowable curvature. The fitness function measures the comprehensive utilization degree of tension and curvature relative to their limits; lower values indicate a higher safety margin and superior overall structural response.

The calculated fitness function curves for the 0° loading direction are shown in Figure 11. As the TDP moves further away (D increases), the fitness function rises, whereas it decreases and eventually stabilizes as the length increment l increases. This phenomenon suggests that when the TDP is closer to the hang-off point, the lazy-wave structure fully utilizes its geometric slack effect, effectively buffering the axial stretching and bending responses caused by longitudinal platform motion and providing a higher safety margin. Regarding the length increment l, once it exceeds a certain threshold, the contribution of additional redundant length to reducing extreme responses diminishes, as evidenced by the stabilization of the fitness function. This indicates that the structural slack capacity has approached saturation. Based on the coupling between cable response and platform motion, a horizontal distance of $D = 2H$ is recommended for the touchdown point. This conclusion is consistent with the findings of Rentschler et al. [15].

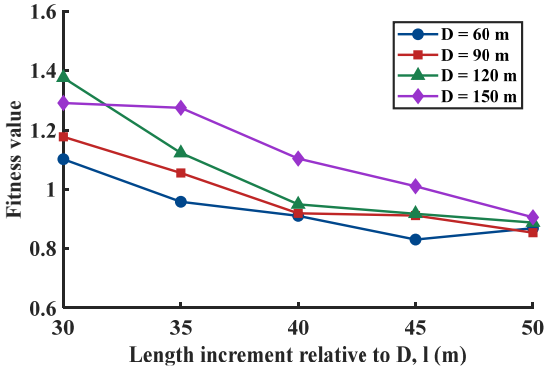


Figure 11. Variation curves of the fitness function under 0° loading direction with respect to touchdown distance D and length increment l.

4.3. PSO-Based Optimization Design

In shallow-water environments, the dynamic response of a lazy-wave dynamic cable is governed not only by the touchdown distance and platform excursions but also significantly by the lengths of the individual cable segments. Building upon the preceding parametric sensitivity analysis, this study introduces the PSO algorithm to perform a multi-objective optimization of the lazy-wave dynamic cable configuration. By constructing a fitness function that integrates structural response characteristics (maximum curvature and maximum tension) with economic indicators (total cable length), a coordinated optimization of safety and cost-effectiveness is achieved.

The specific optimization procedure is as follows. First, a numerical model is established in OrcaFlex, including the floating wind turbine, dynamic cable, and environmental parameters. The lengths of the hang-off section (L_1), buoyancy section (L_2), and touchdown section (L_3) are selected as optimization variables, with ranges of 5–40 m, 5–40 m, and 10–80 m, respectively. Subsequently, the PSO algorithm is initialized with a population size of 50, a maximum iteration count of 100, and a fitness tolerance of 1×10^{-4}, together with the inertia weight, individual learning factor, and social learning factor. Particle positions and velocities are randomly initialized within the variable bounds. For each particle's geometric parameter combination, the solver is automatically invoked via the OrcaFlex Python API to perform static and dynamic time-domain simulations. The maximum tension $T_{\max}$ and maximum curvature $\rho_{\max}$ are extracted from the simulation results. Constraints on cable length, maximum curvature, and maximum tension are handled using a combination of hard constraints and penalty methods. The personal best and global best positions are then updated according to the fitness values, and the iteration process follows the standard PSO velocity and position update formulas. The optimization proceeds until the fitness change over consecutive iterations falls below the tolerance or the maximum number of iterations is reached. Finally, the globally optimal geometric parameters and the corresponding response values are output. The optimization workflow is illustrated in Figure 12.

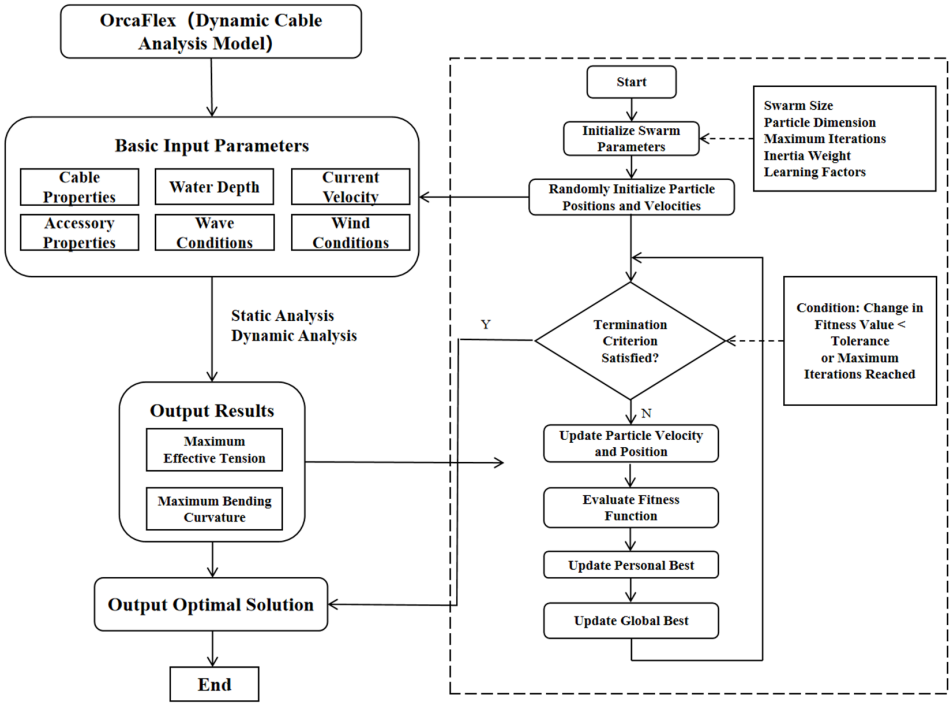


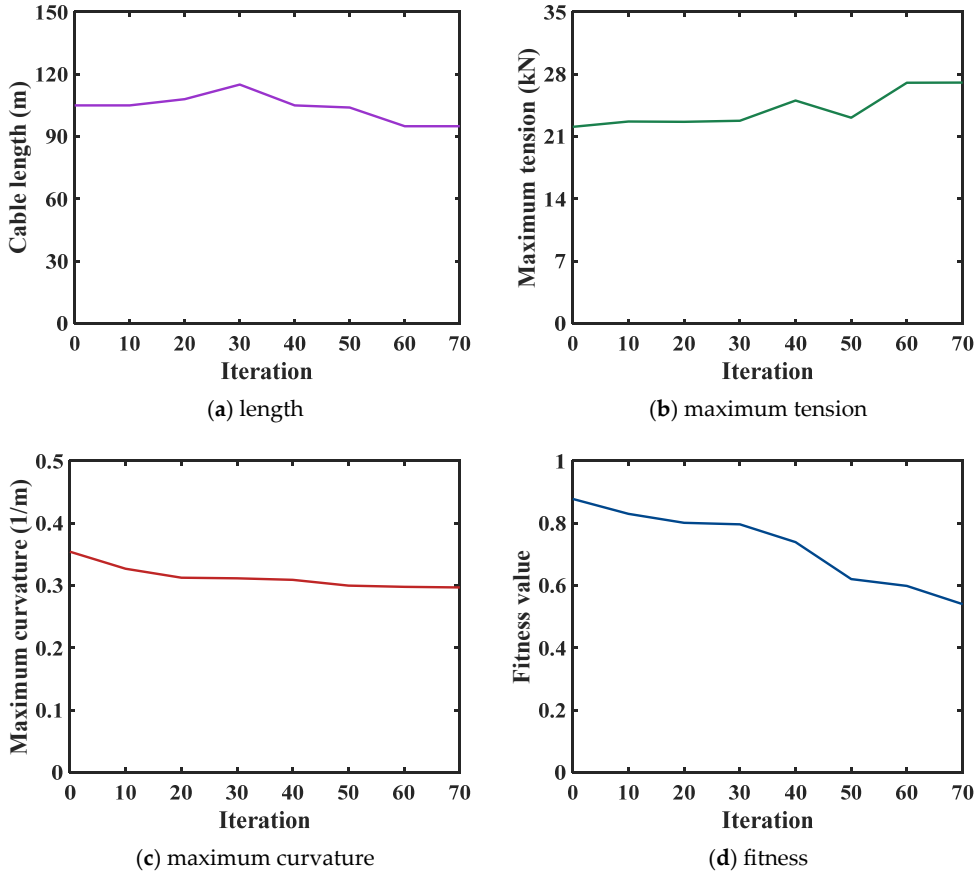
Figure 12. Flowchart of the PSO algorithm for lazy-wave dynamic cable optimization.

The fitness function incorporates the normalized maximum curvature ρ_{max}, maximum tension T_{max}, and total cable length L, as shown in Equation (22).

$$F = \left(\frac{T_{\max}}{T}\right)^{\alpha} + \left(\frac{\rho_{\max}}{\rho}\right)^{\beta} + \left(\frac{1}{L}\right)^{\gamma} \tag{22}$$

where F is the fitness function, α, β, γ represents the weight coefficients reflecting the relative importance of each indicator. T_{max} is the maximum tension from motion analysis, T is the allowable tension, ρ_{max} is the maximum curvature from analysis, and ρ is the allowable curvature. L is the total length of dynamic cables.

Using an initial cable length of 105 m and a horizontal touchdown point distance of 60 m as the baseline, the structural optimization was conducted. The optimization results, shown in Figure 13, demonstrate that, while satisfying all structural safety constraints, the maximum curvature shows a significant downward trend as iterations increase. This indicates that localized bending concentrations are effectively mitigated, and the structural safety margin is substantially improved. In contrast, the maximum tension remains relatively stable and within acceptable limits. Furthermore, the total cable length after optimization is lower than that of the initial design, confirming that the optimized configuration improves dynamic performance while reducing material usage, thereby enhancing economic feasibility.



(**a**) length (**b**) maximum tension

(**c**) maximum curvature (**d**) fitness

Figure 13. Optimization results of the lazy-wave dynamic cable using the PSO algorithm.

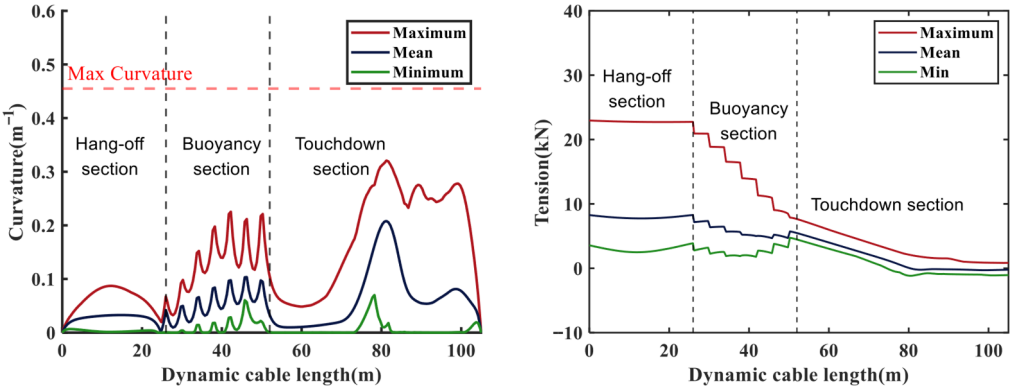
In summary, this optimization successfully lowered the peak curvature and reduced the total cable length without significantly increasing the axial tensile response, demonstrating a robust comprehensive optimization effect.

A comparative analysis of the cable length parameters before and after optimization is provided in Table 9. In this table, L_1 represents the length of the hang-off section, L_2 represents the length of the buoyancy section, L_3 represents the length of the touchdown section, and L represents the total length of the cable. The lengths of the hang-off section and buoyancy section increased slightly, while the touchdown section length and the cable total length (L) were substantially reduced. This suggests that in shallow water, the optimization process improves the geometric buffering capacity to mitigate platform-induced bending concentrations while reducing redundant length in the lower section to minimize material costs.

Table 9. Dynamic cable parameters: before vs. after optimization.

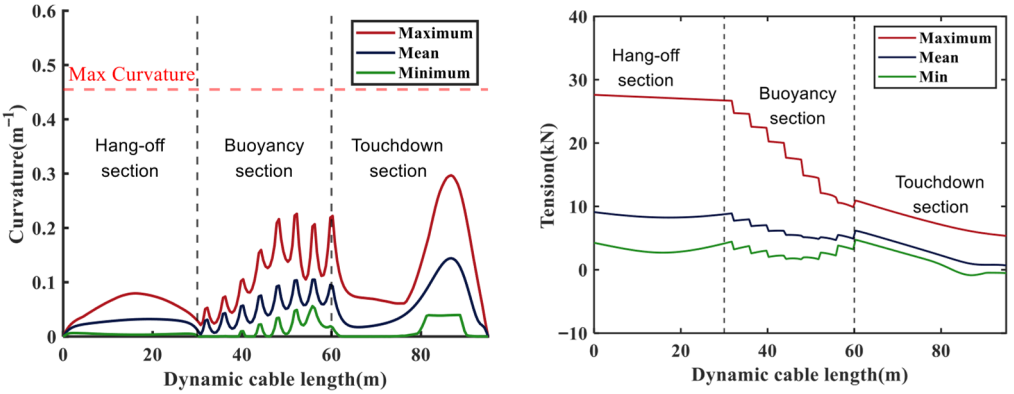
Length	Before Optimization	After Optimization
L_1	26	30
L_2	26	30
L_3	53	35
L	105	95

Further analysis of the curvature and tension distribution along the cable reveals that curvature remains high in the touchdown and buoyancy sections, with the peak curvature consistently occurring in the touchdown section, as shown in Figures 14 and 15, identifying it as the zone most sensitive to bending. Post-optimization, the curvature in the buoyancy section shows a minor decline, while the curvature in the touchdown section is significantly reduced. This suggests that the original design had excessive structural redundancy in the touchdown section, which exacerbated bending concentration; shortening this segment effectively redistributes the bending loads.



(**a**) curvature along cable length (**b**) tension along cable length

Figure 14. Curvature and tension responses of the dynamic cable before optimization.



(**a**) curvature along cable length (**b**) tension along cable length

Figure 15. Curvature and tension responses of the dynamic cable after optimization.

Regarding tension distribution, the maximum tension occurs at the hang-off point and gradually attenuates along the cable length, reflecting that tension is primarily driven by self-weight and platform-induced axial stretching. Following optimization, tension changes in the buoyancy and touchdown sections are negligible, while tension at the hang-off point increases slightly. This occurs because the reduced length of the touchdown section provides less load alleviation for the upper structure, causing a portion of the axial

load to transfer to the hang-off point. Simultaneously, the increased lengths of the hang-off and buoyancy sections redistribute the overall tension.

Ultimately, the optimization primarily improves the bending response distribution by adjusting configuration parameters, with a limited impact on the overall axial tension level. This confirms that curvature is the dominant governing response under these specific operating conditions.

5. Conclusions

This study investigated the dynamic response mechanisms and structural optimization of lazy-wave dynamic power cables under extreme sea states. A coupled numerical model of a floating wind turbine and a dynamic cable was established to systematically reveal the influence of key parameters—specifically environmental loading direction, touchdown point position, and cable length—on tension and curvature responses. Furthermore, a multi-objective optimization method was proposed to balance structural safety with economic feasibility. The primary innovative conclusions are as follows:

Impact of Environmental Loading on Platform Dynamics: The study identified the dominant motion modes of the floating platform under extreme environmental loading and their subsequent influence on the boundary conditions of the dynamic cable. The results show that the 6-DOF responses of the platform exhibit significant directional dependency. Shifting environmental directions causes transitions in the primary motion modes, thereby altering the distribution of axial and transverse force components along the cable. This establishes a clear kinematic foundation for analyzing dynamic cable response mechanisms.

Tension-Curvature Control Mechanisms: The investigation systematically elucidated the governing mechanisms of the tension-curvature response in lazy-wave dynamic cables. The study reveals that, under shallow-water conditions, the 0° loading direction constitutes the governing design case. The touchdown point distance is identified as the primary parameter controlling the axial tension response, while the cable length increment predominantly regulates the bending response level. A recommended value for the touchdown point distance D (relative to the hang-off point) is provided for shallow-water applications.

PSO-Based Optimization Framework: A multi-objective configuration optimization process for lazy-wave dynamic cables was successfully implemented using the Particle Swarm Optimization algorithm. By coupling the numerical model with the optimization algorithm, global search and parameter iteration were achieved under complex nonlinear dynamic conditions. The resulting optimal solution significantly reduced peak curvature and total cable length while satisfying all structural strength constraints. This demonstrates the effectiveness and engineering feasibility of the proposed method under complex environmental loads.

In summary, this study not only clarifies the response characteristics of lazy-wave dynamic cables for floating wind turbines under various loading directions in shallow water but also establishes a multi-objective optimization framework using the Particle Swarm Optimization method. These findings provide a theoretical basis and methodological support for the parameter selection and optimal design of dynamic power cables for large-capacity floating wind turbines in shallow-water environments.

However, future research will focus on the following aspects. Firstly, only three typical loading directions are considered in the current study. Subsequent work should adopt a finer directional interval and also consider the misalignment between wind, wave, and current directions to fully capture the directional sensitivity of the dynamic cable response. Secondly, this study focuses on extreme sea conditions; normal operating condition simulations and time-domain fatigue analysis based on long-term sea state statistics will be carried out to evaluate accumulated fatigue damage. Thirdly, the current optimization ob-

jective function is relatively simple, and the selection of weighting factors lacks sensitivity analysis. Subsequent research will introduce a multi-objective optimization framework and systematically conduct weight sensitivity analysis to enhance the robustness of the optimization results. Finally, the current model can be extended to other cable configurations and different water depths, enabling further investigation of dynamic cables for large-capacity floating wind turbines in shallow water.

Author Contributions: Methodology, M.M.; Validation, M.M.; resources, Y.G.; data curation, M.M.; writing—original draft preparation, M.M.; writing—review and editing, Y.G. All authors have read and agreed to the published version of the manuscript.

Funding: This research received no external funding.

Data Availability Statement: Data are unavailable due to privacy or ethical restrictions but will be provided upon reasonable request.

Conflicts of Interest: The authors declare no conflicts of interest.

References

1. Wang, L.; Hong, Y.; Gao, Y.; Huang, M.; Guo, Z.; Lai, Y.; Zhu, R.; Yang, Q.; He, B. Dynamic catastrophe and control of offshore wind power structures in typhoon environment. *Chin. J. Theor. Appl. Mech.* **2023**, *55*, 567–587.
2. Gielen, D.; Gorini, R.; Wagner, N.; Leme, R.; Gutierrez, L.; Prakash, G.; Asmelash, E.; Janeiro, L.; Gallina, G.; Vale, G. *Global Energy Transformation: A Roadmap to 2050*; International Renewable Energy Agency (IRENA): Abu Dhabi, United Arab Emirates, 2019.
3. Karimirad, M. *Offshore Energy Structures: For Wind Power, Wave Energy and Hybrid Marine Platforms*; Springer: Berlin/Heidelberg, Germany, 2014.
4. Thies, P.R.; Johanning, L.; Smith, G.H. Assessing mechanical loading regimes and fatigue life of marine power cables in marine energy applications. *Proc. Inst. Mech. Eng. Part O J. Risk Reliab.* **2012**, *226*, 18–32. [CrossRef]
5. Warnock, J.; McMillan, D.; Pilgrim, J.; Shenton, S. Failure rates of offshore wind transmission systems. *Energies* **2019**, *12*, 2682. [CrossRef]
6. De Wild, F. *Offshore Wind Industry Joins Forces to Reduce Costs of Cable Failures*; (April 2018 Article); Det Norske Veritas (DNV): Oslo, Norway, 2018.
7. Nasution, F.P.; Sævik, S.; Gjøsteen, J.K. Finite element analysis of the fatigue strength of copper power conductors exposed to tension and bending loads. *Int. J. Fatigue* **2014**, *59*, 114–128. [CrossRef]
8. Martinelli, L.; Lamberti, A.; Ruol, P.; Ricci, P.; Kirrane, P.; Fenton, C.; Johanning, L. Power umbilical for ocean renewable energy systems-feasibility and dynamic response analysis. In Proceedings of the 3rd International Conference on Ocean Energy, Bilbao, Spain, 6–9 October 2010.
9. Zhao, S.; Cheng, Y.; Chen, P.; Nie, Y.; Fan, K. A comparison of two dynamic power cable configurations for a floating offshore wind turbine in shallow water. *AIP. Adv.* **2021**, *11*, 035302. [CrossRef]
10. Beier, D.; Janocha, M.J.; Ye, N.; Ong, M.C. Fatigue assessment of suspended inter-array power cables for floating offshore wind turbines. *Eng. Struct.* **2024**, *308*, 118007. [CrossRef]
11. Ahmad, I.B.; Schnepf, A.; Ong, M.C. An optimization methodology for suspended inter-array power cable configurations between two floating offshore wind turbines. *Ocean. Eng.* **2023**, *278*, 114406. [CrossRef]
12. Guo, Z.; Zhao, X.; Ma, Q.; Li, J.; Wu, Z. Simulation Study on Methods for Reducing Dynamic Cable Curvature in Floating Wind Power Platforms. *J. Mar. Sci. Eng.* **2024**, *12*, 334. [CrossRef]
13. Ericka, L.; Malakonda, R.L.; Leah, S.; Matthew, H. Reference mooring and dynamic cable designs for representative, U.S. floating wind farms. *Ocean Eng.* **2025**, *322*, 120473. [CrossRef]
14. Anna, H.; Martyn, H.; Scott, B.; Shanshan, C.; Robert, R.; Rachel, N.; Tom, T.; Emma, E.; Kieran, M. Experimental–numerical model comparison of a dynamic power cable for a floating offshore wind turbine. *Ocean Eng.* **2025**, *321*, 120384. [CrossRef]
15. Rentschler, M.U.; Adam, F.; Chainho, P.; Krügel, K.; Vicente, P.C. Parametric study of dynamic inter-array cable systems for floating offshore wind turbines. *Mar. Syst. Ocean Technol.* **2020**, *15*, 16–25. [CrossRef]
16. Schnepf, A.; Giljarhus, K.E.T.; Johnsen, Ø.; Lopez-Pavon, C. Dynamic power cable configuration design for floating offshore wind turbines using gradient-based optimization. In *Proceedings of the ASME 2023 42nd International Conference on Ocean, Offshore and Arctic Engineering (OMAE 2023), Melbourne, Australia, 11–16 June 2023*; Volume 8: Ocean Renewable Energy; ASME: New York, NY, USA, 2023; Paper No. OMAE2023-102788, V008T09A037; 11p. [CrossRef]
17. Zhao, X.; Ma, Q.; Li, J.; Wu, Z.; Lu, H.; Xiong, Y. Optimization design of lazy-wave dynamic cable configuration based on machine learning. *J. Mar. Sci. Eng.* **2025**, *13*, 873. [CrossRef]

18. Zhao, B.; Wang, H.; Yan, X.; Wei, Y.; Zhang, C.; Wu, S.; Zhang, D.; Yue, Q. Research on drift limits for floating offshore substations based on the mechanical strength of dynamic cables. *Ocean Eng.* **2026**, *352*, 124514. [CrossRef]
19. Wang, Y.; Yan, F.; Du, Y.; Wang, H.; Ai, S.; Wang, W. A stepwise scheme for the optimization implementation of lazy wave dynamic cables. *Ocean Eng.* **2024**, *311*, 118849. [CrossRef]
20. Gaertner, E.; Rinker, J.; Sethuraman, L.; Zahle, F.; Anderson, B.; Barter, G.; Abbas, N.; Meng, F.; Bortolotti, P.; Skrzypinski, W.; et al. *Definition of the IEA 15-Megawatt Offshore Reference Wind Turbine*; National Renewable Energy Laboratory (NREL): Golden, CO, USA, 2020; 44p.
21. Allen, C.; Viscelli, A.; Dagher, H.; Goupee, A.; Gaertner, E.; Abbas Hall, M.; Barter, G. *Definition of the UMaine VolturnUS-S Reference Platform Developed for the IEA Wind 15-Megawatt Offshore Reference Wind Turbine: IEA Wind TCP Task 37*; National Wind Technology Center: Golden, CO, USA, 2020; 41p.
22. Li, Y.; Gao, Y.; Wang, L. Numerical study on mooring system failure effects of floating offshore wind turbines in medium-shallow water. *Ocean. Eng.* **2025**, *43*, 101–115.
23. Liu, S.; Li, J.; Xu, J.; Wang, C.; Tian, C.; Zou, P.; Zhu, W.; Wang, Y.; Du, B. Current Carrying Capacity of 66kV Wind Turbine Cable with High Thermal Conductivity. In Proceedings of the IEEE 4th International Conference on Electrical Materials and Power Equipment (ICEMPE), Shanghai, China, 7–10 May 2023; pp. 1–4.
24. CIGRE. *CIGRE TB 862 Recommendations for Mechanical Testing of Submarine Cables for Dynamic Applications*; CIGRE: Paris, France, 2022.
25. CIGRE. *CIGRE TB 623 Recommendations for Mechanical Testing of Submarine Cables*; CIGRE: Paris, France, 2015.
26. Liu, H.; Zhang, X.; Tu, L. A modified particle swarm optimization using adaptive strategy. *Expert Syst. Appl.* **2020**, *152*, 113353. [CrossRef]
27. DNV. *Design of Offshore Steel Structures, General-LRFD Method, DNVGL-OS-C101*; DNV: Oslo, Norway, 2018.
28. DNV. *Environmental Conditions and Environmental Loads, DNV-RP-C205*; DNV: Oslo, Norway, 2010.

Disclaimer/Publisher's Note: The statements, opinions and data contained in all publications are solely those of the individual author(s) and contributor(s) and not of MDPI and/or the editor(s). MDPI and/or the editor(s) disclaim responsibility for any injury to people or property resulting from any ideas, methods, instructions or products referred to in the content.